Weierstraß-Institut

für Angewandte Analysis und Stochastik

Leibniz-Institut im Forschungsverbund Berlin e. V.

Preprint ISSN 2198-5855

Improved dual meshes using Hodge-optimized triangulations for electromagnetic problems

Rainer Schlundt

submitted: September 21, 2015

Weierstrass Institute
Mohrenstr. 39
10117 Berlin
Germany
E-Mail: rainer.schlundt@wias-berlin.de

No. 2156
Berlin 2015

2010 *Mathematics Subject Classification.* 35Q61, 65F10, 65F15, 65N22, 65N50.

Key words and phrases. Optimal triangulations, discrete Hodge star, Maxwell's equations, finite integration technique, microcell method, linear algebraic equations.

Edited by
Weierstraß-Institut für Angewandte Analysis und Stochastik (WIAS)
Leibniz-Institut im Forschungsverbund Berlin e. V.
Mohrenstraße 39
10117 Berlin
Germany

Fax: +49 30 20372-303
E-Mail: preprint@wias-berlin.de
World Wide Web: http://www.wias-berlin.de/

Abstract

Hodge-optimized triangulations (HOT) can optimize the dual mesh alone or both the primal and dual meshes. They make them more self-centered while keeping the primal-dual orthogonality. The weights are optimized in order to improve one or more of the discrete Hodge stars. Using the example of Maxwell's equations we consider academic examples to demonstrate the generality of the approach.

1 Introduction

First we start with the definition of a k-simplex. A k-simplex σ^k is the convex hull of $k+1$ geometrically independent points $\mathbf{x_1}, \ldots, \mathbf{x_{k+1}} \in \mathbb{R}^d$ with $d \in \{0,1,2,3\}$ and $0 \leq k \leq d$.

$$\sigma^k = \left\{ \mathbf{z} \in \mathbb{R}^d \,:\, \mathbf{z} = \sum_{i=1}^{k+1} \lambda_i \mathbf{x_i} \,,\, 0 \leq \lambda_i \leq 1 \,,\, \sum_{i=1}^{k+1} \lambda_i = 1 \right\} \tag{1}$$

Any simplex spanned by a proper subset of $\{\mathbf{x_1}, \ldots, \mathbf{x_{k+1}}\}$ is called a face of σ^k. The union of the proper faces of σ^k is called its boundary. The interior of σ^k is the set difference of σ^k and its boundary. The interior of σ^0 is σ^0. The volume of σ^k is denoted by $|\sigma^k|$. Define $|\sigma^0|$ = 1 (cf. [7]). Given a set of points $S \subset \mathbb{R}^d$. For $d = 3$, the triangulation $\mathcal{T}(S)$ of this set of points is a set of tetrahedra (cf. [19]). Each k-simplex is associated with a dual $(d-k)$-cell, $*\sigma^k$, $k \in \{0,1,2,3\}$ (cf. [10]). The dual of $\mathcal{T}$ forms a cell complex $\mathcal{D}$. If the initial triangulation is Delaunay then this dual is simply the Voronoi diagram of the primal vertices. Thus, we obtain a primal-dual triangulation $(\mathcal{T}, \mathcal{D})$ with the nice properties of non-self-intersection, convexity, and orthogonality of the primal-dual elements (cf. [9]). The triangulations $(\mathcal{T}, \mathcal{D})$ don't allow to change the dual mesh if the primary is fixed. The complex $(\mathcal{RT}, \mathcal{PD})$ is a generalization of $(\mathcal{T}, \mathcal{D})$ and provides orthogonal primal-dual triangulations with much more self-centered simplices σ^d. The regular triangulation $\mathcal{RT}$ (weighted Delaunay triangulation) is a generalization of $\mathcal{T}$ and the power diagrams $\mathcal{PD}$ (Laguerre or weighted Voronoi diagrams) are the dual structures of $\mathcal{RT}$.

Each point $\mathbf{x_i} \in \mathbb{R}^d$ in $\mathcal{RT}$ is associated with a real number (weight) $w_i \in \mathbb{R}$ and $(\mathbf{x_i}, w_i)$ is called as weighted point. The power distance of a point $\mathbf{z} \in \mathbb{R}^d$ with respect to a weighted point $(\mathbf{x_i}, w_i)$ is defined as

$$\pi_i(\mathbf{z}) = \|\mathbf{z} - \mathbf{x_i}\|_2^2 - w_i \tag{2}$$

and it doesn't matter whether $\mathbf{z}$ is weighted or unweighted. Two weighted points $(\mathbf{x_i}, w_i)$ and $(\mathbf{x_j}, w_j)$ are said to be orthogonal if $\|\mathbf{x_j} - \mathbf{x_i}\|^2 = w_i + w_j$, i.e., $\pi_i(\mathbf{x_j}) = w_j$. For each weighted point $(\mathbf{x_i}, w_i)$ with $\mathbf{x_i} \in S$, its power cell is defined by

$$\tilde{V}_i = \{\mathbf{z} \in \mathbb{R}^d \,:\, \pi_i(\mathbf{z}) \leq \pi_j(\mathbf{z}), \forall \mathbf{x_j} \in S\} \,. \tag{3}$$

More information on weighted Voronoi cells and the relation between regular triangulations in $\mathbb{R}^d$ and convex hulls in $\mathbb{R}^{d+1}$ can be found in [9, 13, 19].

The weighted circumcenter, also called the orthogonal center, of a k-simplex σ^k is computed by

$$\mathbf{c}(\sigma^k) = \mathbf{x_l} + \frac{1}{2k!|\sigma^k|} \sum_{\mathbf{x_j} \in \sigma^k} (\|\mathbf{x_l} - \mathbf{x_j}\|^2 + w_l - w_j)\hat{\mathbf{n}}_\mathbf{j}^k \tag{4}$$

where $\mathbf{x_l}$ is any of the vertices of σ^k and $\hat{\mathbf{n}}_\mathbf{j}^k$ denotes the inward-pointing normal of the face of σ^k opposite to $\mathbf{x_j}$ (cf. [9]). For this, the orientation of the d-simplex σ^d, i.e., the orientation of the set of $d+1$ points is important. It is positive if the points occure in the orientation illustrated

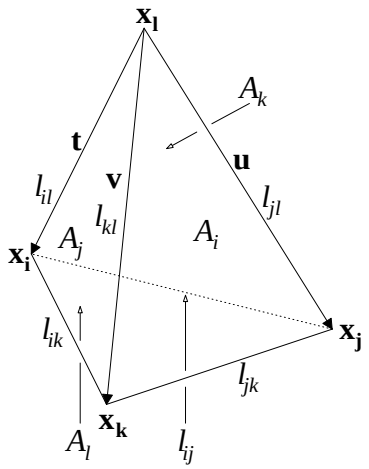

Figure 1: A tetrahedron having positive orientation.

in Fig. 1. We can apply a right-hand rule: orient the right hand with fingers curled to follow the circular sequence jkl. If the thumb points toward i then σ^d has a positive orientation. In other words, the vectors $\mathbf{t}$, $\mathbf{u}$, and $\mathbf{v}$, in this order, define a positive frame. Using Eq. 4, we obtain for the orthogonal center $\mathbf{c_{ijkl}}$ the following expression in $\mathbb{R}^3$ (cf. [13]):

$$\mathbf{c_{ijkl}} = \mathbf{x_l} + \frac{(\|\mathbf{t}\|^2 + w_l - w_i)\hat{\mathbf{n}}_\mathbf{i} + (\|\mathbf{u}\|^2 + w_l - w_j)\hat{\mathbf{n}}_\mathbf{j} + (\|\mathbf{v}\|^2 + w_l - w_k)\hat{\mathbf{n}}_\mathbf{k}}{12|T_{ijkl}|} \tag{5}$$

where $|T_{ijkl}|$ is the volume of the tetrahedron T_{ijkl} spanned by the vertices $\mathbf{x_i}$, $\mathbf{x_j}$, $\mathbf{x_k}$, and $\mathbf{x_l}$. Using $\mathbf{t} = \mathbf{x_i} - \mathbf{x_l}$, $\mathbf{u} = \mathbf{x_j} - \mathbf{x_l}$, and $\mathbf{v} = \mathbf{x_k} - \mathbf{x_l}$, the outward-pointing and inward-pointing normals are

$$\begin{aligned}
\mathbf{n_i} &= \mathbf{v} \times \mathbf{u}, & \hat{\mathbf{n}}_\mathbf{i} &= -\mathbf{n_i} = \mathbf{u} \times \mathbf{v}, \\
\mathbf{n_j} &= \mathbf{t} \times \mathbf{v}, & \hat{\mathbf{n}}_\mathbf{j} &= -\mathbf{n_j} = \mathbf{v} \times \mathbf{t}, \\
\mathbf{n_k} &= \mathbf{u} \times \mathbf{t}, & \hat{\mathbf{n}}_\mathbf{k} &= -\mathbf{n_k} = \mathbf{t} \times \mathbf{u}, \quad \text{and} \\
\mathbf{n_l} &= (\mathbf{x_i} - \mathbf{x_k}) \times (\mathbf{x_j} - \mathbf{x_k}).
\end{aligned} \tag{6}$$

An alternative formula for the last vector is $\mathbf{n_l} = \hat{\mathbf{n}}_\mathbf{i} + \hat{\mathbf{n}}_\mathbf{j} + \hat{\mathbf{n}}_\mathbf{k}$. A simplex σ^k is said to be self-centered if $\mathbf{c}(\sigma^k)$ lies in the interior of σ^k.

2 Hodge-optimized triangulations

For an arbitrary primal element σ, the diagonal approximation of the Hodge star of a continuous differential form α is given by the relation

$$\frac{1}{|*\sigma|}\int_{*\sigma}\star\alpha \approx \frac{1}{|\sigma|}\int_{\sigma}\alpha\,, \tag{7}$$

where $|\sigma|$ and $|*\sigma|$ are the volumes of these elements (cf. [9, 14]). Using Eq. (7) the error density e_i on the dual of a k-simplex σ_i^k is given as the average difference between the discrete approximation and the exact Hodge star:

$$e_i = \frac{1}{|*\sigma_i^k|}\left|\frac{|*\sigma_i^k|}{|\sigma_i^k|}\int_{\sigma_i^k}\alpha - \int_{*\sigma_i^k}\star\alpha\right| = \left|\frac{1}{|\sigma_i^k|}\int_{\sigma_i^k}\alpha - \frac{1}{|*\sigma_i^k|}\int_{*\sigma_i^k}\star\alpha\right|. \tag{8}$$

One can assemble a total error by summing the error densities e_i over local regions, specific to σ_i^k and $*\sigma_i^k$. These regions denoted as $\diamond(\sigma_i^k \cup *\sigma_i^k)$ are the convex hulls of σ_i^k and $*\sigma_i^k$ (cf. [9, 10]).

$$E_2(\mathcal{RT},\mathcal{PD},\star^k) = \left(\sum_{\sigma_i^k}\int_{\diamond(\sigma_i^k\cup *\sigma_i^k)} e_i^2\right)^{\frac{1}{2}} = \left(\sum_{\sigma_i^k}\frac{|\sigma_i^k||*\sigma_i^k|}{\binom{d}{k}}e_i^2\right)^{\frac{1}{2}}. \tag{9}$$

Using the Wasserstein metric W_2 the following estimate is a useful bound of (9):

$$E_2(\mathcal{RT},\mathcal{PD},\star^k)^2 \leq \frac{1}{\binom{d}{k}}\sum_{\sigma_i^k}|\sigma_i^k||*\sigma_i^k|W_2(\sigma_i^k,*\sigma_i^k)^2 \equiv \star^k - \mathsf{HOT}_{2,2}(\mathcal{RT},\mathcal{PD})\,. \tag{10}$$

2.1 General minimization procedure

A HOT mesh consists of a regular triangulation $\mathcal{RT}$ and its associated power diagram $\mathcal{PD}$ for which $\mathcal{RT}$, $\mathcal{PD}$, or both have been optimized in order to reduce one HOT functional. A pseudocode of a general procedure is given in Table 1. This common minimization procedure works without anything else but an evaluation of a HOT energy and its gradient which will derive in closed form from direct integration.
Information about the solution of the unconstrained minimization problem

$$\min_{\mathbf{x}\in\mathbb{R}^n} f(\mathbf{x})$$

with the Wolfe conditions for some smooth $f:\mathbb{R}^n \longrightarrow \mathbb{R}$ can be found in [10]. The solution of the minimization problem occurs without updating the complex $(\mathcal{RT},\mathcal{PD})$.

2.2 HOT_{22} energies

The $\mathsf{HOT}_{2,2}$ energies can be expressed as a function of signed distances between the weighted circumcenters of k- and $(k+1)$-simplices with $0 \leq k \leq d-1$ (cf. Fig. 2). The weighted

Table 1: Basic pseudocode of HOT mesh optimization.

Input: vertices $\{\mathbf{x_i}^0\}$ with weights $\mathbf{w}^0 = \{w_i^0\}$ and
$0 \leq k \leq d$ (type of $\star^k - \text{HOT}_{2,2}(\mathcal{RT}, \mathcal{PD})$)
Compute $(\mathcal{RT}, \mathcal{PD})$
do $m = 1, \ldots, n_w$
Compute $\star^k - \text{HOT}_{2,2}(\mathcal{RT}, \mathcal{PD})$
do $l = 1, \ldots, n_x(m)$
Pick step direction $\mathbf{d}_x$ for $\star^k - \text{HOT}_{2,2}(\mathcal{RT}, \mathcal{PD})$
Find α satisfying Wolfe conditions
$\mathbf{x_i}^{l+1} := \mathbf{x_i}^l + \alpha\, \mathbf{d}_x$
Update $(\mathcal{RT}, \mathcal{PD})$
end (l)
Pick step direction $\mathbf{d}_w$ for $\star^k - \text{HOT}_{2,2}(\mathcal{RT}, \mathcal{PD})$
Find β satisfying Wolfe conditions
$\mathbf{w}^{m+1} := \mathbf{w}^m + \beta\, \mathbf{d}_w$
Update $(\mathcal{RT}, \mathcal{PD})$
end (m)

circumcenter of the k-simplex σ^k is the orthogonal projection of the weigthted circumcenter of the $(k+1)$-simplex σ^{k+1} onto simplex σ^k. The signed distance from the weighted circumcenter of σ^{k+1}, c_{k+1}, to the weighted circumcenter of σ^k has a positive distance if the simplices σ^{k+1} and $\{\sigma^k, c_{k+1}\}$ have the same orientation, and negative otherwise.

For both $\star^0$ and $\star^d$, $\text{HOT}_{2,2}$ energies can be easily computed by splitting d-cells $*\sigma^0$ or primal d-simplices σ^d into canonical subsimplices for which closed form integral expressions $W(\mathbf{p}, T)$ are found. T is a tetrahedron spanned by the edges a, b, and c and vertex $\mathbf{p}$ is adjacent to edge

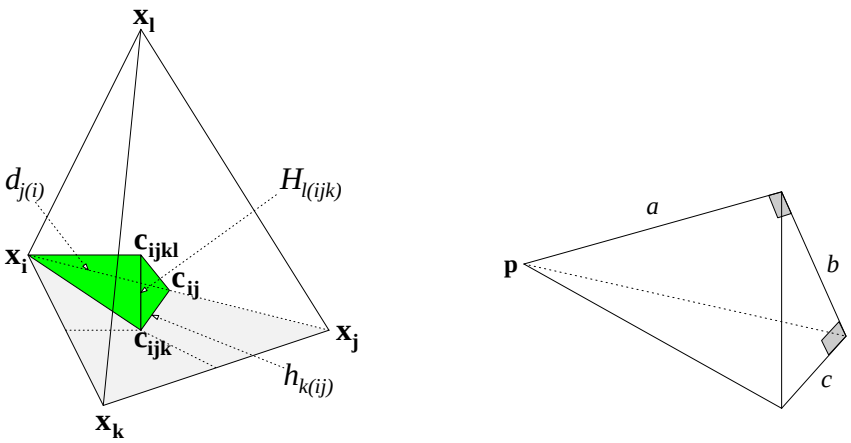

Figure 2: Signed distances between circumcenters.

a (cf. Fig. 2). Using the squared distance in Eq. (10) the integral expression $W(\mathbf{p}, T)$ is given by:

$$W(\mathbf{p}, T) = \int_0^a \int_0^{\frac{b}{a}x} \int_0^{\frac{c}{b}y} (x^2 + y^2 + z^2) dz dy dx = \frac{1}{5}\Big(\frac{a^3bc}{2} + \frac{ab^3c}{4} + \frac{abc^3}{12}\Big) . \quad (11)$$

Using Eq. (11) and $\mathbf{p} \longleftarrow \mathbf{c_{ijkl}}$, $a \longleftarrow H_{l(ijk)}$, $b \longleftarrow h_{k(ij)}$, and $c \longleftarrow d_{j(i)}$ the $\star^3 - \mathsf{HOT}_{2,2}$ energy for every tetrahedron T_{ijkl} is expressed as a function of the signed distances $d_{j(i)}$, $h_{k(ij)}$, and $H_{l(ijk)}$ between circumcenters as follows:

$$\star^3 - \mathsf{HOT}_{2,2}(T_{ijkl}) = \sum_r \sum_s \sum_t \frac{1}{5}\left(\frac{H^3_{r(stu)} h_{s(tu)} d_{t(u)}}{2} + \frac{H_{r(stu)} h^3_{s(tu)} d_{t(u)}}{4} + \frac{H_{r(stu)} h_{s(tu)} d^3_{t(u)}}{12}\right)$$

where the indices r, s, t, and u are determined by $r \in \{i, j, k, l\}$, $s \in \{i, j, k, l\}\backslash\{r\}$, $t \in \{i, j, k, l\}\backslash\{r, s\}$, and $u \in \{i, j, k, l\}\backslash\{r, s, t\}$. The arrangement of the indices s, t, and u of $H_{r(stu)}$ and t and u of $h_{s(tu)}$, respectively is not of any importance. Every permutation of $\{s, t, u\}$ yields the same distance $H_{r(\dots)}$. The same applies to $\{t, u\}$ and $h_{s(\dots)}$.
Thus, the total error (10) is computed by

$$E_2(\mathcal{RT}, \mathcal{PD}, \star^3)^2 = \sum_{T_{ijkl}} \star^3 - \mathsf{HOT}_{2,2}(T_{ijkl}) .$$

Detailed information to the other remaining stars can be found in [10].

The signed distances $d_{j(i)}$, $h_{k(ij)}$, and $H_{l(ijk)}$ between (weighted) circumcenters $\mathbf{c_i}$ ($= \mathbf{x_i}$) and $\mathbf{c_{ij}}$, $\mathbf{c_{ij}}$ and $\mathbf{c_{ijk}}$, and $\mathbf{c_{ijk}}$ and $\mathbf{c_{ijkl}}$ are given by (cf. [9, 10]):

$$d_{j(i)} = \frac{\ell_{ij}^2 + w_i - w_j}{2\ell_{ij}} , \quad \ell_{ij} = \|x_j - x_i\| , \quad (12a)$$

$$h_{k(ij)} = \frac{\ell_{ij} \cot \gamma_k}{2} + \frac{w_j \cot \gamma_i + w_i \cot \gamma_j}{2\ell_{ij}} - \frac{w_k \ell_{ij}}{4|t_{ijk}|} , \quad (12b)$$

$$H_{l(ijk)} = (\mathbf{c_{ijk}} - \mathbf{c_{ijkl}}) \cdot \frac{(\mathbf{x_i} - \mathbf{x_k}) \times (\mathbf{x_j} - \mathbf{x_k})}{\|(\mathbf{x_i} - \mathbf{x_k}) \times (\mathbf{x_j} - \mathbf{x_k})\|} \quad (12c)$$

$$= \begin{cases} \|\mathbf{c_{ijk}} - \mathbf{c_{ijkl}}\| & \text{if } \mathbf{x_l} \text{ and } \mathbf{c_{ijkl}} \text{ lie in the same half-plane} \\ -\|\mathbf{c_{ijk}} - \mathbf{c_{ijkl}}\| & \text{otherwise} . \end{cases} \quad (12d)$$

γ_i is the angle at $\mathbf{x_i}$ in triangle t_{ijk} spanned by the vertices $\mathbf{x_i}$, $\mathbf{x_j}$, and $\mathbf{x_k}$.

2.2.1 Weight optimization

The weight optimization of each $\mathsf{HOT}_{2,2}$ energy can easily done using the derivatives of Eq. (12):

$$\frac{\partial d_{j(i)}}{\partial w_i} = \frac{1}{2\ell_{ij}} , \quad \frac{\partial d_{j(i)}}{\partial w_j} = -\frac{1}{2\ell_{ij}} ,$$

$$\frac{\partial h_{k(ij)}}{\partial w_i} = \frac{\cot\gamma_j}{2\ell_{ij}}\,, \quad \frac{\partial h_{k(ij)}}{\partial w_j} = \frac{\cot\gamma_i}{2\ell_{ij}}\,, \quad \frac{\partial h_{k(ij)}}{\partial w_k} = -\frac{\ell_{ij}}{4|t_{ijk}|}\,,$$

$$\begin{aligned}\frac{\partial H_{l(ijk)}}{\partial w_s} &= \left(\frac{\partial \mathbf{c_{ijk}}}{\partial w_s} - \frac{\partial \mathbf{c_{ijkl}}}{\partial w_s}\right) \cdot \frac{(\mathbf{x_i}-\mathbf{x_k})\times(\mathbf{x_j}-\mathbf{x_k})}{\|(\mathbf{x_i}-\mathbf{x_k})\times(\mathbf{x_j}-\mathbf{x_k})\|} \\ &= -\frac{1}{12|T_{ijkl}|}\mathbf{n_s^3}\cdot\frac{(\mathbf{x_i}-\mathbf{x_k})\times(\mathbf{x_j}-\mathbf{x_k})}{\|(\mathbf{x_i}-\mathbf{x_k})\times(\mathbf{x_j}-\mathbf{x_k})\|} \\ &= \mp\frac{1}{12|T_{ijkl}|}\mathbf{n_s^3}\cdot\frac{(\mathbf{c_{ijk}}-\mathbf{c_{ijkl}})}{\|\mathbf{c_{ijk}}-\mathbf{c_{ijkl}}\|}\,, \quad s\in\{i,j,k,l\}\,.\end{aligned}$$

The derivative of the weighted circumcenter with respect to the weights at vertex $\mathbf{x_l}$ result in

$$\frac{\partial \mathbf{c_{ijk}}}{\partial w_r} = \frac{1}{4|t_{ijk}|}\mathbf{n_r^2}\,, \quad \frac{\partial \mathbf{c_{ijk}}}{\partial w_l} \equiv 0\,, \quad \text{and} \quad \frac{\partial \mathbf{c_{ijkl}}}{\partial w_s} = \frac{1}{12|T_{ijkl}|}\mathbf{n_s^3}$$

where $r\in\{i,j,k\}$, $s\in\{i,j,k,l\}$, and $\mathbf{n_r^2}$ and $\mathbf{n_s^3}$ denote the outward normals of the triangle t_{ijk} and of the tetrahedron T_{ijkl}, respectively. The normal $\frac{(\mathbf{x_i}-\mathbf{x_k})\times(\mathbf{x_j}-\mathbf{x_k})}{\|(\mathbf{x_i}-\mathbf{x_k})\times(\mathbf{x_j}-\mathbf{x_k})\|}$ is perpendicular to $\mathbf{n_r^2}$. The same applies for the normal $\frac{(\mathbf{c_{ijk}}-\mathbf{c_{ijkl}})}{\|\mathbf{c_{ijk}}-\mathbf{c_{ijkl}}\|}$.

2.2.2 Vertex position optimization

The derivatives of the signed distances between (weighted) circumcenters with respect to the vertices for Eq. (12a) are given by

$$\begin{aligned}\frac{\partial d_{j(i)}}{\partial \mathbf{x_i}} &= \frac{(\mathbf{x_j}-\mathbf{x_i})^T}{2}\left(\frac{w_i-w_j}{\ell_{ij}^3} - \frac{1}{\ell_{ij}}\right) \qquad \text{and} \\ \frac{\partial d_{j(i)}}{\partial \mathbf{x_j}} &= \frac{(\mathbf{x_j}-\mathbf{x_i})^T}{2}\left(\frac{1}{\ell_{ij}} - \frac{w_i-w_j}{\ell_{ij}^3}\right) = -\frac{\partial d_{j(i)}}{\partial \mathbf{x_i}}\,.\end{aligned}$$

Using Phytagoras' theorem, one can differentiate the signed distance $h_{k(ij)}$ (12b) between circumcenters $\mathbf{c_{ij}}$ and $\mathbf{c_{ijk}}$ in a triangle t_{ijk} with respect to $\mathbf{x_i}$.

$$\begin{aligned}\|\mathbf{x_i}-\mathbf{c_{ijk}}\|^2 &= \|\mathbf{c_{ij}}-\mathbf{c_{ijk}}\|^2 + \|\mathbf{x_i}-\mathbf{c_{ij}}\|^2 \\ h_{k(ij)}^2 &= \|\mathbf{x_i}-\mathbf{c_{ijk}}\|^2 - d_{j(i)}^2 \\ \mathbf{x_i}-\mathbf{c_{ijk}} &= \frac{1}{4|t_{ijk}|}\sum_{r\in\{j,k\}}(\|\mathbf{x_i}-\mathbf{x_r}\|^2 + w_i - w_r)\mathbf{n_r}^2 \qquad \text{by (4)}\end{aligned}$$

For the triangle t_{ijk} with $|t_{ijk}| = \frac{1}{2}\|(\mathbf{x_i}-\mathbf{x_j})\times(\mathbf{x_i}-\mathbf{x_k})\|$ we get

$$\frac{\partial |t_{ijk}|}{\partial \mathbf{x_i}} = \frac{1}{4|t_{ijk}|}((\mathbf{x_i}-\mathbf{x_j})\times(\mathbf{x_i}-\mathbf{x_k}))^T\cdot(I\times(\mathbf{x_j}-\mathbf{x_k})).$$

We finally obtain the following expression:

$$\frac{\partial h_{k(ij)}}{\partial \mathbf{x_i}} = \frac{1}{h_{k(ij)}}\left((\mathbf{x_i}-\mathbf{c_{ijk}})^T\frac{\partial(\mathbf{x_i}-\mathbf{c_{ijk}})}{\partial \mathbf{x_i}} - d_{j(i)}\frac{\partial d_{j(i)}}{\partial \mathbf{x_i}}\right). \qquad (13)$$

Similar formulas as Eq. (13) can be derived for $\frac{\partial h_{k(ij)}}{\partial \mathbf{x_j}}$ and $\frac{\partial h_{k(ij)}}{\partial \mathbf{x_k}}$, respectively.

Using Phytagoras' theorem twice, one can differentiate the signed distance $H_{l(ijk)}$ (12c),(12d) between circumcenters $\mathbf{c_{ijk}}$ and $\mathbf{c_{ijkl}}$ in a tetrahedron T_{ijkl} with respect to $\mathbf{x_i}$.

$$\begin{aligned}
\|\mathbf{x_i} - \mathbf{c_{ijkl}}\|^2 &= \|\mathbf{c_{ijk}} - \mathbf{c_{ijkl}}\|^2 + \|\mathbf{x_i} - \mathbf{c_{ijk}}\|^2 \\
&= \|\mathbf{c_{ijk}} - \mathbf{c_{ijkl}}\|^2 + \|\mathbf{c_{ij}} - \mathbf{c_{ijk}}\|^2 + \|\mathbf{x_i} - \mathbf{c_{ij}}\|^2 \\
H_{l(ijk)}^2 &= \|\mathbf{x_i} - \mathbf{c_{ijkl}}\|^2 - (h_{k(ij)}^2 + d_{j(i)}^2) \\
\mathbf{x_i} - \mathbf{c_{ijkl}} &= \frac{1}{12|T_{ijkl}|} \sum_{r\in\{j,k,l\}} (\|\mathbf{x_i} - \mathbf{x_r}\|^2 + w_i - w_r)\mathbf{n_r}^2 \qquad \text{by (4)}
\end{aligned}$$

For the tetrahedron T_{ijkl} with $|T_{ijkl}| = \frac{1}{6}|((\mathbf{x_i} - \mathbf{x_j}) \times (\mathbf{x_i} - \mathbf{x_k})) \cdot (\mathbf{x_i} - \mathbf{x_l})|$ we get

$$\frac{\partial |T_{ijkl}|}{\partial \mathbf{x_i}} = \frac{1}{6} \frac{((\mathbf{x_i} - \mathbf{x_j}) \times (\mathbf{x_i} - \mathbf{x_k})) \cdot (\mathbf{x_i} - \mathbf{x_l})}{|((\mathbf{x_i} - \mathbf{x_j}) \times (\mathbf{x_i} - \mathbf{x_k})) \cdot (\mathbf{x_i} - \mathbf{x_l})|} \cdot \\ \big(((\mathbf{x_j} - \mathbf{x_k}) \times (\mathbf{x_i} - \mathbf{x_l}))^T + ((\mathbf{x_i} - \mathbf{x_j}) \times (\mathbf{x_i} - \mathbf{x_k}))^T\big).$$

We finally obtain the following expression:

$$\frac{\partial H_{l(ijk)}}{\partial \mathbf{x_i}} = \frac{1}{H_{l(ijk)}} \left((\mathbf{x_i} - \mathbf{c_{ijkl}})^T \frac{\partial (\mathbf{x_i} - \mathbf{c_{ijkl}})}{\partial \mathbf{x_i}} - \left(h_{k(ij)} \frac{\partial h_{k(ij)}}{\partial \mathbf{x_i}} + d_{j(i)} \frac{\partial d_{j(i)}}{\partial \mathbf{x_i}} \right) \right). \quad (14)$$

Similar formulas as Eq. (14) can be derived for $\frac{\partial H_{l(ijk)}}{\partial \mathbf{x_j}}$, $\frac{\partial H_{l(ijk)}}{\partial \mathbf{x_k}}$, and $\frac{\partial H_{l(ijk)}}{\partial \mathbf{x_l}}$.

3 Maxwellian grid equations

We consider the Maxwell's equations in integral form. We obtain in vector notation the following equations:

$$\begin{aligned}
&\oint_P \mathbf{E} \cdot \mathrm{d}\mathbf{l} = -\frac{\partial}{\partial t} \iint_A \mathbf{B} \cdot \mathrm{d}\mathbf{A} \qquad \oint_P \mathbf{H} \cdot \mathrm{d}\mathbf{l} = \frac{\partial}{\partial t} \iint_A \mathbf{D} \cdot \mathrm{d}\mathbf{A} + \iint_A \mathbf{J} \cdot \mathrm{d}\mathbf{A} \\
&\oiint_S \mathbf{B} \cdot \mathrm{d}\mathbf{S} = 0 \qquad\qquad \oiint_S \mathbf{D} \cdot \mathrm{d}\mathbf{S} = \iiint_V q \, \mathrm{d}V \,.
\end{aligned} \quad (15)$$

The constitutive relations belonging to them are

$$\mathbf{D} = \varepsilon \, \mathbf{E} \,, \qquad \mathbf{B} = \mu \, \mathbf{H} \,, \qquad \mathbf{J} = \kappa \, \mathbf{E} \,. \quad (16)$$

Here, A is a surface with boundary curve P, V is a volume bounded by a surface S, and q is the volume charge density.

3.1 Discretization of Maxwell's equations

Given a set $S \subset \mathbb{R}^3$ of n_p points $\mathbf{x_i} = \sigma_i^0$, $i = 1, \ldots, n_p$, and associated weights $w_i \in \mathbb{R}$. The regular triangulation $\mathcal{RT}(S)$ consists of n_r 3-simplices (tetrahedra) σ_i^3, $i = 1, \ldots, n_r$, n_f faces $A_i = \sigma_i^2$, $i = 1, \ldots, n_f$, and n_e edges $L_i = \sigma_i^1$, $i = 1, \ldots, n_e$. The power diagram $\mathcal{PD}$ consists of n_r 0-cells, $*\sigma_i^3$, i.e., the weighted orthogonal centers of σ_i^3, of n_f edges $\tilde{L}_i$, $*\sigma_i^2$, n_e faces $\tilde{A}_i$, $*\sigma_i^1$, and n_p 3-cells, $*\sigma_i^0$.

Using FIT [16, 17, 8, 3, 4, 5, 10], the electric and magnetic voltages and fluxes over the elemtary objects of σ_i^3 and $*\sigma_i^0$ are defined as state variables in the following way:

$$
\begin{aligned}
e_i &= \int_{L_i} \mathbf{E} \cdot \mathrm{d}\mathbf{l} & h_j &= \int_{\tilde{L}_j} \mathbf{H} \cdot \mathrm{d}\mathbf{l} & i &= 1, \ldots, n_e \\
d_i &= \iint_{\tilde{A}_i} \mathbf{D} \cdot \mathbf{n}\, \mathrm{d}\mathbf{A} & b_j &= \iint_{A_j} \mathbf{B} \cdot \mathbf{n}\, \mathrm{d}\mathbf{A} & j &= 1, \ldots, n_f \\
j_i &= \iint_{\tilde{A}_i} \mathbf{J} \cdot \mathbf{n}\, \mathrm{d}\mathbf{A} & q_k &= \iiint_{\tilde{V}_k} q\, \mathrm{d}V & k &= 1, \ldots, n_p\,.
\end{aligned}
$$

where $\mathbf{n}$ is the outward-pointing normal of the faces A_j and $\tilde{A}_i$, respectively. The Maxwell's equations (cf. (15)) can then discretized for all the components [18]. Thus, we obtain a compact matrix-vector form:

$$
\begin{aligned}
C\,\mathbf{e} &= -\frac{d}{dt}\mathbf{b}\,, & \tilde{C}\,\mathbf{h} &= \frac{d}{dt}\mathbf{d} + \mathbf{j}\,, \\
S\,\mathbf{b} &= 0\,, & \tilde{S}\,\mathbf{d} &= \mathbf{q}\,.
\end{aligned}
\tag{17}
$$

The matrices C, $C := (c_{ij})_{n_f \times n_e}$, and $\tilde{C}$, $\tilde{C} := (\tilde{c}_{ij})_{n_e \times n_f}$, represent the incidence relations between edges and faces on $\mathcal{RT}$ and $\mathcal{PD}$, respectively. Analogously, the matrices S, $S := (s_{ij})_{n_r \times n_f}$, and $\tilde{S}$, $\tilde{S} := (\tilde{s}_{ij})_{n_p \times n_e}$, represent the incidence relations between faces and volumes on $\mathcal{RT}$ and $\mathcal{PD}$, respectively. The matrices C, $\tilde{C}$, S, and $\tilde{S}$ satisfy the important relations

$$
\tilde{C} = C^T, \quad S\,C = 0, \quad \text{and} \quad \tilde{S}\,\tilde{C} = 0\,.
$$

3.2 Discretization of the constitutive relations

To complete the system of equations (17), the quantities defined on the primary grid and the quantities defined on the dual grid are connected by the Hodge star operator, $\star$, (cf. [3, 15]):

$$
D = \varepsilon \star E, \quad B = \mu \star H, \quad J = \kappa \star E\,. \tag{18}
$$

The Hodge operator depends on a metric. If the metric is taken to be the permittivity, the permeability, or the conductivity tensor, the constitutive relations (18) become

$$
D = M_\varepsilon\, E, \quad B = M_\mu\, H, \quad J = M_\kappa\, E\,. \tag{19}
$$

Let σ_i^k be the i-th k-simplex and $*\sigma_i^k$ the dual $(d-k)$-cell of the primal-dual triangulation $(\mathcal{RT}, \mathcal{PD})$. Then the discrete k-th Hodge star is a diagonal matrix M^k with

$$(M^k)_{ij} = \frac{|*\sigma_i^k|}{|\sigma_i^k|}\delta_{ij}\,, \quad \forall i, \forall j\,. \tag{20}$$

Thus, using (20) we get

$$(M_\varepsilon)_{ii} = \frac{\bar{\varepsilon}\tilde{A}_i}{L_i}\,, \quad (M_\nu)_{ii} = \frac{\bar{\nu}\tilde{L}_i}{A_i}\,, \quad \text{and} \quad (M_\kappa)_{ii} = \frac{\bar{\kappa}\tilde{A}_i}{L_i}\,, \tag{21}$$

where $\bar{\varepsilon}$ is the face-averaged permittivity, $\bar{\nu}$ the edge-averaged reluctivity ($\nu = \mu^{-1}$), and $\bar{\kappa}$ the face-averaged conductivity. If the weighted circumcenter of any simplex σ_i^d is outside the simplex, i.e., σ_i^d is not self-centered, then the matrices M_ε, M_ν, and M_κ (cf. (21)) are not positive definite. This is an important disadvantage.

For each simplex σ_i^d that is not self-centered we use a locally barycentric dual mesh to make the matrices M_ε, M_ν, and M_κ symmetric positive definite. The construction of the constitutive matrices is performed using the microcell method (cf. [5, 10]). Microcells are elementary cells with hexahedral shape in the 3d cases. Each primary tetrahedral cell is divided by the dual edges in four different microcells, one for each of its four nodes (cf. [10]). The interpolation method starts from the assumption of a homogeneous medium and a constant field in the microcells (cf. [4, 5]). The global matrices M_ε, M_ν, and M_κ can be assembled from associated local matrices of the microcells (cf. [10]).

Another more widely used approach for barycentric dual meshes employs Whitney forms in the definition of the discrete Hodge star. Whitney k-forms are piecewise linear functions on a primal mesh. For a tetrahedron (Fig. 1), we use ordered indexing of nodes to denote the vertices (e.g. $\sigma^0 = [\mathbf{x_i}]$), oriented edges (e.g. $\sigma^1 = [\mathbf{x_i}, \mathbf{x_j}]$), oriented faces (e.g. $\sigma^2 = [\mathbf{x_i}, \mathbf{x_j}, \mathbf{x_k}]$), and oriented cells (e.g. $\sigma^3 = [\mathbf{x_i}, \mathbf{x_j}, \mathbf{x_k}, \mathbf{x_l}]$). In terms of vector proxies (cf. [3]), we have

$$\begin{aligned}
&\eta_{\sigma^0} = \lambda_i && \text{(Whitney } 0\text{-form)}\\
&\eta_{\sigma^1} = \lambda_i\nabla\lambda_j - \lambda_j\nabla\lambda_i && \text{(Whitney } 1\text{-form)}\\
&\eta_{\sigma^2} = 2(\lambda_i\nabla\lambda_j\times\nabla\lambda_k + \lambda_j\nabla\lambda_k\times\nabla\lambda_i + \lambda_k\nabla\lambda_i\times\nabla\lambda_j) && \text{(Whitney } 2\text{-form)}\\
&\eta_{\sigma^3} = 1/|\sigma^3| \text{ on } \sigma^3, 0 \text{ elsewhere} && \text{(Whitney } 3\text{-form)}
\end{aligned} \tag{22}$$

where λ_i (cf. Eq. (1)) is the barycentric function for the vertex, i.e., $\lambda_i(\mathbf{x_j}) = \delta_{ij}$. Using (22), we obtain

$$(M^{k,Whit})_{ij} = \int_\Omega \eta_{\sigma_i^k}\cdot\eta_{\sigma_j^k}dV\,. \tag{23}$$

$M^{k,Whit}$ is called the Galerkin Hodge. On a locally barycentric dual mesh we use Galerkin Hodges (23) based on Whitney edge and face elements on tetrahedron to obtain analogous formulas as (21):

$$\begin{aligned}
&(M_\varepsilon^{Whit})_{ij} = \int_\Omega \varepsilon\,\eta_{\sigma_i^1}\cdot\eta_{\sigma_j^1}dV\,, \qquad (M_\nu^{Whit})_{ij} = \int_\Omega \nu\,\eta_{\sigma_i^2}\cdot\eta_{\sigma_j^2}dV\,,\\
&(M_\kappa^{Whit})_{ij} = \int_\Omega \kappa\,\eta_{\sigma_i^1}\cdot\eta_{\sigma_j^1}dV\,.
\end{aligned} \tag{24}$$

3.3 Linear algebraic equations in the frequency domain

From Sec. 3.1, the equation for the fast varying transient electromagnetic fields is

$$C^T M_\nu C\mathbf{e} + M_\kappa \frac{d}{dt}\mathbf{e} + M_\varepsilon \frac{d^2}{dt^2}\mathbf{e} = 0\,.$$

If all field quantities vary sinusoidally with time, with angular frequency ω, the electric field $\mathbf{E}(r,t)$ may be written as:

$$\mathbf{E}(r,t) = \Re\big(\underline{\mathbf{E}(r)} e^{\jmath\omega t}\big)\,.$$

We get Maxwell's equations in phasor form:

$$\begin{aligned} C\underline{\mathbf{e}} &= -\jmath\omega\underline{\mathbf{b}} \\ C^T M_\nu \underline{\mathbf{b}} &= \quad \jmath\omega M_\varepsilon \underline{\mathbf{e}} + M_\kappa \underline{\mathbf{e}}\,. \end{aligned} \tag{25}$$

We obtain the eigenvalue problem

$$C^T M_\nu C\underline{\mathbf{e}} + \jmath\omega M_\kappa \underline{\mathbf{e}} = \omega^2 M_\varepsilon \underline{\mathbf{e}}$$

and without lossy materials ($M_\kappa = 0$) the problem

$$C^T M_\nu C\underline{\mathbf{e}} = \omega^2 M_\varepsilon \underline{\mathbf{e}}\,.$$

Using

$$\underbrace{\tilde{S}C^T}_{=0} M_\nu C\underline{\mathbf{e}} = \omega^2 \tilde{S} M_\varepsilon \underline{\mathbf{e}} = \omega^2 \tilde{S}\underline{\mathbf{d}} = 0 \quad \text{and} \quad M_\varepsilon \tilde{S}^T D_{\tilde{V}}^{-1} \tilde{S} M_\varepsilon \underline{\mathbf{e}} \equiv 0$$

we obtain the boundary value problem

$$(C^T M_\nu C + M_\varepsilon \tilde{S}^T D_{\tilde{V}}^{-1} \tilde{S} M_\varepsilon - \omega^2 M_\varepsilon)\underline{\mathbf{e}} = 0 \tag{26}$$

where $D_{\tilde{V}}$ is the diagonal matrix of dual cell volumes $\tilde{V}$ ($*\sigma^0$). Taking into account the boundary conditions, Eq. (26) yields the form $Ax = b$. Using independent set orderings, the permutations P_i transform the matrix A_i with $A_0 = A$ into the form

$$A_i \quad \longrightarrow \quad P_i A_i P_i^T = \begin{pmatrix} D_i & E_i^T \\ E_i & H_i \end{pmatrix}$$

where D_i is a diagonal, E_i, and H_i are sparse matrices. We get the factorized system of linear equations

$$\begin{pmatrix} I_i & 0 \\ E_i D_i^{-1} & I_i \end{pmatrix} \begin{pmatrix} D_i & E_i^T \\ 0 & H_i - E_i D_i^{-1} E_i^T \end{pmatrix} \begin{pmatrix} y_{i,1} \\ y_{i,2} \end{pmatrix} = \begin{pmatrix} c_{i,1} \\ c_{i,2} \end{pmatrix} \tag{27}$$

with $y_i = P_i x_i = (y_{i,1}, y_{i,2})^T$ and $c_i = P_i b_i = (c_{i,1}, c_{i,2})^T$. Using Krylov subspace methods, (27) can be solved iteratively (cf. [11, 12]).

4 Numerical results

We consider four academic examples to demonstrate the generality of the approach. The ability to optimize weights to improve the dual structure is very useful. Moving vertices of a primal mesh is potentially harmful, as it affects the surface shape. Therefore, only internal points are considered for optimization. For the four examples we compute the inverse of the matrix M_ε to show the change of number of nonzero entries of M_ε^{-1}.
We use a stable iterative method for computing an approximate inverse of a square sparse matrix A as follows:

$$P_{n+1} = P_n(2I - AP_n), \quad n = 0, 1, 2, \ldots,$$

under the condition $\|I - AP_0\| < 1$. Then $P_n \to A^{-1}$ as $n \to \infty$.

The primal triangular mesh is generated using REGTET, a Fortran program for computing a regular tetrahedralization for a finite set of weighted points in 3d space (cf. [1, 2]). It is based on an algorithm by Edelsbrunner and Shah for constructing regular tetrahedralizations with incremental topological flipping (cf. [6]).

Example 1. The first example has the form of a crystal (cf. Fig. 3). The colored areas represent different material parameters. We define a rectangular regular grid on the surface of a rectangular polyhedron that contains the set of input points $\{\mathbf{x_1}, \ldots, \mathbf{x_8}\}$ to become, together with this set of input points, the set for which a tetrahedralization is to be computed. For $n_{add} \geq 2$ for each facet of the polyhedron a set of $n_{add} \times n_{add}$ points is generated. This set defines a rectangular regular grid and contains the four vertices of the facet. The union of the six sets thus generated define the rectangular grid on the surface of the polyhedron with n_{pol} points:

$$n_{pol} = 6(n_{add} - 2)^2 + 12(n_{add} - 2) + 8 = 6n_{add}^2 - 12n_{add} + 8\,.$$

In Table 2 #tet denotes the number of all tetrahedra and #sctet the number of self-centered tetrahedra. The weights of the input points and the weights of the points on the surface of the rectangular polyhedron are $w_i = 0.00$. The finished weights for $n_{add} = 0$ at the end of the iteration are given in Fig. 3. This set of weights is not unique. However the number of self-centered tetrahedra has increased significantly.

Table 2: The number of self-centered tetrahedra for $\star^3 - \mathrm{HOT}_{2,2}$ (Example 1).

n_{add}	$(\mathcal{T}, \mathcal{D})$			$(\mathcal{RT}, \mathcal{PD})$ at first			$(\mathcal{RT}, \mathcal{PD})$ finished		
	#tet	#sctet	%	#tet	#sctet	%	#tet	#sctet	%
0	12	0	0.00	12	0	0.00	12	10	83.33
2	48	0	0.00	48	0	0.00	47	20	42.55
3	95	14	14.74	95	14	14.74	83	59	71.08
4	170	50	29.41	170	50	29.41	165	116	70.30
5	277	48	17.33	277	48	17.33	269	166	61.71

In Table 3, the dimension n_e and the number of nonzero entries of the matrices M_ε and M_ε^{-1} are shown. While the weights of the input points in Table 4 are also $w_i = 0.00$, the weights

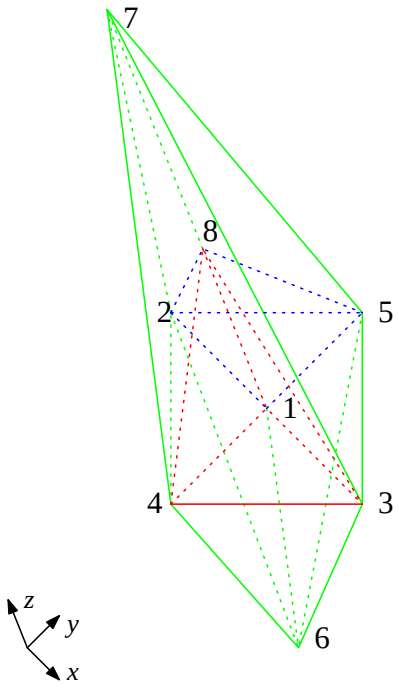

$$\mathbf{x_1} = (\ 0.0,\ \ 0.0,\ \ 0.0)$$
$$\mathbf{x_2} = (-1.0,\ \ 0.0,\ \ 0.0)$$
$$\mathbf{x_3} = (\ 1.0,\ \ 0.0,\ \ 0.0)$$
$$\mathbf{x_4} = (\ 0.0, -1.0,\ \ 0.0)$$
$$\mathbf{x_5} = (\ 0.0,\ \ 1.0,\ \ 0.0)$$
$$\mathbf{x_6} = (-0.5, -0.5, -1.0)$$
$$\mathbf{x_7} = (\ 0.0,\ \ 0.0,\ \ 2.0)$$
$$\mathbf{x_8} = (\ 0.0,\ \ 0.0,\ \ 1.0)$$

	w_i at first	w_i finished
1	0.00	−0.005075
2	0.00	0.477244
3	0.00	0.716525
4	0.00	0.477620
5	0.00	0.729235
6	0.00	0.746571
7	0.00	1.859071
8	0.00	0.065864

Figure 3: The crystal.

Table 3: The number of nonzero entries of M_ε and M_ε^{-1} (Example 1).

n_{add}	$(\mathcal{RT}, \mathcal{PD})$ at first			$(\mathcal{RT}, \mathcal{PD})$ finished		
	n_e	M_ε	M_ε^{-1}	n_e	M_ε	M_ε^{-1}
0	23	167	529	23	67	83
2	69	673	4 761	68	484	2 480
3	152	1 176	21 908	139	511	4 561
4	287	2 135	76 739	282	1 124	23 640
5	478	3 560	228 484	470	2 020	75 474

Table 4: The number of self-centered tetrahedra for $\star^3 - \mathrm{HOT}_{2,2}$ in dependence of the weights on the surface points (Example 1).

n_{add}	$(\mathcal{RT}, \mathcal{PD})$ at first			$(\mathcal{RT}, \mathcal{PD})$ finished		
	#tet	#sctet	%	#tet	#sctet	%
2	48	0	0.00	47	20	42.55
3	99	15	15.15	92	58	63.04
4	167	46	27.54	164	115	70.12
5	284	9	3.17	261	144	55.17

on the surface are $w_i = 1.00$. The iterative behavior between $w_i = 0.00$ and $w_i = 1.00$ on the surface of the polyhedron is different. This example has no internal points for vertex position optimization.

Example 2. The second example is a rectangular bar that is crossed by another bar (cf. Fig. 4). As in the first example, here too the colored areas represent different material parameters. In

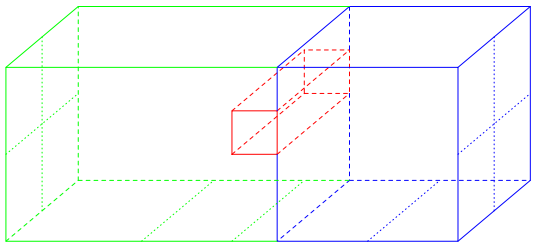

Figure 4: A rectangular bar that is crossed by anaother rectangular bar.

Table 5, the numbers of self-centered tetrahedra are shown both in dependence of the weights of the input points and vertex/weight optimization. The weights of the input points are changed as a function of the terms

$$\begin{aligned} & i \pmod 8 \cdot 0.10, && (\bar{w}) \\ & i \pmod 8 \cdot 0.12, && (\tilde{w}) \\ \text{and} \quad & i \pmod 9 \cdot 0.08, && (\hat{w}) \end{aligned}$$

respectively. Also in this example, the iterative behavior is different in dependence of the weights of the input points.

Table 5: The number of self-centered tetrahedra for $\star^3 - \mathrm{HOT}_{2,2}$ both in dependence of the weights of the input points and vertex/weight optimization (Example 2).

$(\mathcal{RT}, \mathcal{PD})$ at first			$(\mathcal{RT}, \mathcal{PD})$ finished (weight optim.)			$(\mathcal{RT}, \mathcal{PD})$ finished (vertex/weight optim.)			w_i
#tet	#sctet	%	#tet	#sctet	%	#tet	#sctet	%	
144	4	2.78	141	112	79.43	143	109	76.22	0
141	48	34.04	141	106	75.18	141	99	70.21	$\bar{w}$
141	49	34.75	135	101	74.81	138	97	70.29	$\tilde{w}$
144	36	25.00	142	102	71.83	144	113	78.47	$\hat{w}$

In Table 6, the number of nonzero entries of the matrices M_ν, M_ε, and M_ε^{-1} are shown. The values n_e and n_f are the dimensions of the material matrices M_ε and M_ν, respectively. In Fig. 5 this matrices are shown with no weights of input points. The term n_{nz} represents the number of nonzero elements of M_ε and M_ν, respectively. Except for the initialization $w_i \leftarrow \hat{w}$, the weight optimization yields better results than the vertex position/weight optimization.

Table 6: The number of nonzero entries of M_ν, M_ε, and M_ε^{-1} (Example 2).

$(\mathcal{RT}, \mathcal{PD})$ at first			$(\mathcal{RT}, \mathcal{PD})$ finished (weight optim.)			$(\mathcal{RT}, \mathcal{PD})$ finished (vertex/weight optim.)			w_i
n_e	M_ε	M_ε^{-1}	n_e	M_ε	M_ε^{-1}	n_e	M_ε	M_ε^{-1}	
255	1 829	65 025	250	648	5 242	254	716	13 238	0
252	1 210	60 032	250	654	14 056	252	838	14 534	$\bar{w}$
252	1 214	57 612	242	646	13 814	249	851	12 539	$\tilde{w}$
255	1 415	62 007	253	709	13 017	255	757	8 367	$\hat{w}$
n_f	M_μ		n_f	M_μ		n_f	M_μ		
340	1 834		333	637		338	710		0
334	1 352		333	703		334	800		$\bar{w}$
334	1 336		320	690		328	792		$\tilde{w}$
340	1 510		336	772		340	686		$\hat{w}$

Example 3. The third example is a grid of points over the interior of a cube in 3d space with edge lengths $[1, 5] \times [1, 6] \times [1, 7]$. In each coordinate direction, the grid uses 5 points. These points are equally spaced. Thus, the number of vertices equals 125. In Table 7, the numbers of self-centered tetrahedra are shown both in dependence of the weights of the input points and vertex/weight optimization. In Table 8, the number of nonzero entries of the matrices M_ν, M_ε, and M_ε^{-1} are shown.

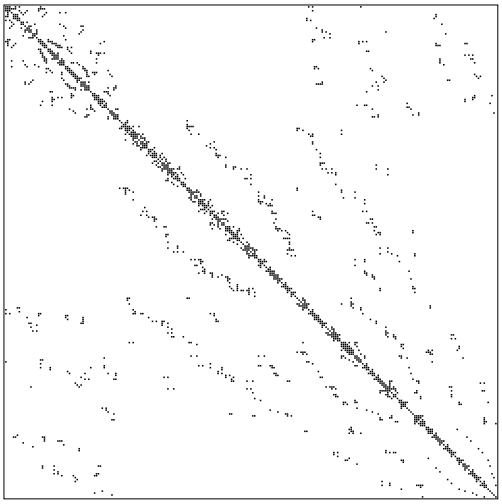

(a) M_ε (at first): $n_e = 255, n_{nz} = 1829$

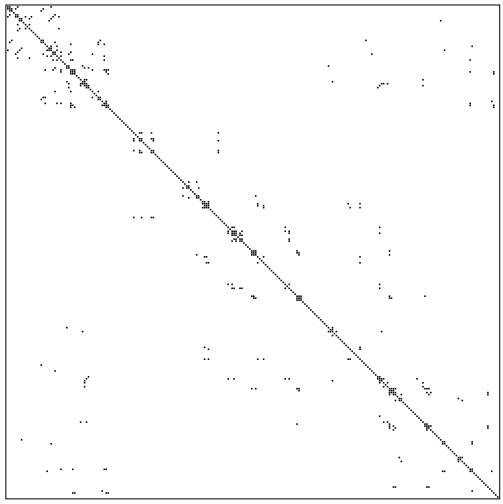

(b) M_ε (finished): $n_e = 250, n_{nz} = 648$

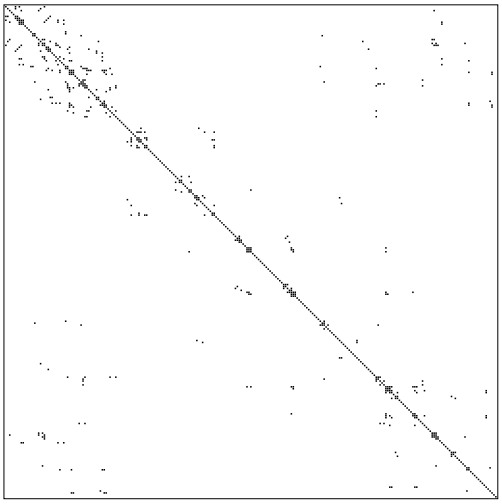

(c) M_ν (at first): $n_f = 340, n_{nz} = 1834$

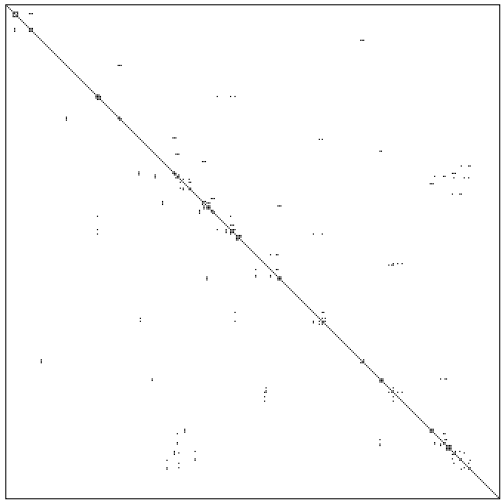

(d) M_ν (finished): $n_f = 333, n_{nz} = 637$

Figure 5: The nonzero pattern of matrices M_ε and M_ν.

Example 4. The fourth example is a grid of points over the interior of a tetrahedron in 3d. The grid is defined by specifying the coordinates of an enclosing tetrahedron. The coordinates are $(0, 0, 0)$, $(10, 0, 0)$, $(0, 10, 0)$, and $(0, 0, 10)$. Each edge of the tetrahedron is devided in 5 subintervals. Thus, the number of vertices equals 56. In Table 9, the numbers of self-centered tetrahedra are shown both in dependence of the weights of the input points and vertex/weight optimization. In Table 10, the number of nonzero entries of the matrices M_ν, M_ε, and M_ε^{-1} are shown.

Table 7: The number of self-centered tetrahedra for $\star^3 - \mathrm{HOT}_{2,2}$ both in dependence of the weights of the input points and vertex/weight optimization (Example 3).

$(\mathcal{RT}, \mathcal{PD})$ at first			$(\mathcal{RT}, \mathcal{PD})$ finished (weight optim.)			$(\mathcal{RT}, \mathcal{PD})$ finished (vertex/weight optim.)			w_i
#tet	#sctet	%	#tet	#sctet	%	#tet	#sctet	%	
384	0	0.00	370	313	84.59	359	308	85.79	0
384	87	22.66	365	275	75.34	361	317	87.81	$\bar{w}$
384	88	22.92	366	247	67.49	319	208	65.20	$\tilde{w}$
384	93	24.22	369	284	76.96	372	287	77.15	$\hat{w}$

Table 8: The number of nonzero entries of M_ν, M_ε, and M_ε^{-1} (Example 3).

$(\mathcal{RT}, \mathcal{PD})$ at first			$(\mathcal{RT}, \mathcal{PD})$ finished (weight optim.)			$(\mathcal{RT}, \mathcal{PD})$ finished (vertex/weight optim.)			w_i
n_e	M_ε	M_ε^{-1}	n_e	M_ε	M_ε^{-1}	n_e	M_ε	M_ε^{-1}	
604	4 850	364 816	586	1 286	24 110	579	1 599	15 211	0
604	3 954	349 294	581	1 737	48 399	577	1 467	15 325	$\bar{w}$
604	3 990	344 586	582	2 092	115 872	515	2 411	90 057	$\tilde{w}$
604	3 666	346 936	587	1 609	42 553	591	2 231	80 457	$\hat{w}$
n_f	M_μ		n_f	M_μ		n_f	M_μ		
864	4 958		834	1 432		814	1 408		0
864	4 082		824	1 822		816	1 340		$\bar{w}$
864	4 062		826	2 126		725	2 025		$\tilde{w}$
864	3 998		833	1 741		840	1 850		$\hat{w}$

Table 9: The number of self-centered tetrahedra for $\star^3 - \mathrm{HOT}_{2,2}$ both in dependence of the weights of the input points and vertex/weight optimization (Example 4).

$(\mathcal{RT}, \mathcal{PD})$ at first			$(\mathcal{RT}, \mathcal{PD})$ finished (weight optim.)			$(\mathcal{RT}, \mathcal{PD})$ finished (vertex/weight optim.)			w_i
#tet	#sctet	%	#tet	#sctet	%	#tet	#sctet	%	
124	1	0.81	118	77	65.25	118	83	70.34	0
122	35	28.69	115	76	66.09	115	80	69.57	$\bar{w}$
122	35	28.69	115	77	66.96	109	77	70.64	$\tilde{w}$
120	42	35.00	112	97	86.61	118	92	77.97	$\hat{w}$

5 Conclusions

A combination of a mainly orthogonal and locally barycentric mesh is used to discretize the Maxwell's equations in integral form using FIT. The constitutive relations are discretized using

Table 10: The number of nonzero entries of M_ν, M_ε, and M_ε^{-1} (Example 4).

$(\mathcal{RT}, \mathcal{PD})$ at first			$(\mathcal{RT}, \mathcal{PD})$ finished (weight optim.)			$(\mathcal{RT}, \mathcal{PD})$ finished (vertex/weight optim.)			w_i
n_e	M_ε	M_ε^{-1}	n_e	M_ε	M_ε^{-1}	n_e	M_ε	M_ε^{-1}	
229	1 609	52 441	217	777	18 149	219	821	14 499	0
227	1 167	45 413	214	734	12 358	214	750	9 486	$\bar{w}$
227	1 167	45 413	214	716	12 314	206	698	5 072	$\tilde{w}$
225	1 029	44 535	213	433	1 391	223	645	6 657	$\hat{w}$
n_f	M_μ		n_f	M_μ		n_f	M_μ		
298	1 640		283	733		284	688		0
294	1 276		277	715		277	681		$\bar{w}$
294	1 276		277	693		264	624		$\tilde{w}$
290	1 170		272	432		286	578		$\hat{w}$

the Hodge star operator. It relates differential forms of different degrees. The duality between regular triangulations and power diagrams allows a different choice on the dual mesh once the primal mesh is fixed. For each tetrahedron that is not self-centered we construct the constitutive matrices by using the microcell method. The Hodge-optimized triangulation strategy makes more self-centered tetrahedra and thus improved one or more of the discrete Hodge stars. Due to efficiency reasons the set of weights and vertices/weights, respectively is a non-optimal minimum. However, using the weight optimization, the number of non-zero elements of the material matrices is important reduced. The vertex position optimization alone hardly improved the dual meshes. An open problem is the construction of the inverse of the material matrix M_ε.

References

[1] Javier Bernal. Lexicographical manipulations for correctly computing regular tetrahedralizations with incremental topological flipping. NISTIR 6335, 1999.

[2] Javier Bernal. REGTET: A program for computing regular tetrahedralizations. NISTIR 6786, 2001.

[3] A. Bossavit. Discretization of electromagnetic problems: The "generalized finite differecesäpproach. In W.H.A. Schilders and E.J.W. ter Maten, editors, *Numerical Methods in Electromagnetics*, volume XIII of *Handbook of numerical analysis*, pages 443–522. Elsevier, Amsterdam, 2005.

[4] M. Cinalli, F. Edelvik, R. Schumann, and T. Weiland. Consistent material operators for tetrahedral grids based on geometrical principles. *International Journal of Numerical Modelling: Electronic Networks, Devices and Fields*, 17(5):487–507, 2004.

[5] Marco Cinalli and Andrea Schiavoni. A stable and consistent generalization of the FDTD technique to nonorthogonal unstructured grids. *IEEE Transactions on Antennas and Propagations*, 54(5):1503–1512, 2006.

[6] H. Edelsbrunner and N.R. Shah. Incremental topological flipping works for regular triangulations. *Algorithmica*, 15(3):223–241, 1996.

[7] A. Gillette. Notes on discrete exterior calculus. Technical report, University of Texas at Austin, 2009.

[8] R. Hiptmair. Finite elements in computational electromagnetism. *Acta Numerica*, 11:237–339, 2002.

[9] Patrick Mullen, Pooran Memari, Fernando Goes, and Mathieu Desbrun. HOT: Hodge-optimized triangulations. *ACM Transactions on Graphics*, 30(4), 2011.

[10] Rainer Schlundt. Regular triangulation and power diagrams for Maxwell's equations. WIAS Preprint No. 2017, Weierstraß-Institut für Angewandte Analysis und Stochastik, 2014.

[11] Rainer Schlundt, Franz-Josef Schückle, and Wolfgang Heinrich. Shifted linear systems in electromagnetics. Part I: Systems with identical right-hand sides. WIAS Preprint No. 1420, Weierstraß-Institut für Angewandte Analysis und Stochastik, 2009.

[12] Rainer Schlundt, Franz-Josef Schückle, and Wolfgang Heinrich. Shifted linear systems in electromagnetics. Part II: Systems with multiple right-hand sides. WIAS Preprint No. 1646, Weierstraß-Institut für Angewandte Analysis und Stochastik, 2011.

[13] Jonathan Richard Shewchuk. Lecture notes on geometric robustness. University of California at Berkeley, 2013.

[14] A. Stern, Y. Tong, M. Desbrun, , and J.E. Marsden. Geometric computational electrodynamics with variational integrators and discrete differential forms. arXiv:0707.4470v3 [math.NA], 2009.

[15] K.F. Warnick, R.H. Selfridge, and D.V. Arnold. Teaching electromagnetic field theory using differential forms. *IEEE Transactions on Education*, 40, No. 1:53–68, 1997.

[16] T. Weiland. A discretization method for the solution of Maxwell's equations for six-component fields. *Electronics and Communication (AEÜ)*, 31:116–120, 1977.

[17] T. Weiland. On the unique numerical solution of Maxwellian eigenvalue problems in three dimensions. *Particle Accelerators (PAC)*, 17:277–242, 1985.

[18] T. Weiland. Time domain electromagnetic field computation with finite difference methods. *International Journal of Numerical Modelling: Electronic Networks, Devices and Fields*, 9(4):295–319, 1996.

[19] Michal Zemek. Regular triangulation in 3d and its applications. Technical Report No. DCSE/TR-2009-03, University of West Bohemia, 2009.